Journal of *Marine Science and Engineering*

MDPI

Article

Control Optimization Method for Ship Direct Current Microgrid Based on Impedance Reshaping

Weiqiang Liao [1,2,3], Xin Dong [1], Rongfeng Yang [1,2,*] and Zhongfei Qiao [1]

[1] School of Marine Engineering, Jimei University, Xiamen 361021, China; wq_liao@jmu.edu.cn (W.L.); 202211824001@jmu.edu.cn (X.D.); 202212855074@jmu.edu.cn (Z.Q.)
[2] Marine Engineering College and Key Laboratory of Fujian Province Marine and Ocean Engineering, Jimei University, Xiamen 361021, China
[3] Innovation Laboratory for Sciences and Technologies of Energy Materials of Fujian Province, Xiamen 361021, China
* Correspondence: yangrf@jmu.edu.cn

Abstract: In response to the constant power negative impedance characteristics on the load side of a ship DC microgrid, leading to voltage oscillation issues in the DC bus, this paper proposes a control optimization method based on impedance reshaping using bus voltage feedback. First, a simplified small-signal diagram of a lithium battery energy storage system converter is analyzed. Combining active damping control technology, an impedance regulator is introduced, and its parameters are optimized to effectively reduce the output impedance magnitude on the power source side. Subsequently, a ship DC microgrid simulation model is constructed using MATLAB R2022a/Simulink for validation, and comparative analysis is conducted on the anti-interference ability of the DC bus voltage before and after impedance reshaping. Finally, a model is built on a semi-physical simulation platform to experimentally verify the proposed method. The research results indicate that the proposed control optimization method can effectively increase the system's stability margin, suppress DC bus oscillations, and enhance the anti-interference ability of the ship DC microgrid's bus voltage when facing significant power load variations.

Keywords: ship DC microgrid; impedance reshaping; bus voltage feedback; control optimization; stability margin

Citation: Liao, W.; Dong, X.; Yang, R.; Qiao, Z. Control Optimization Method for Ship Direct Current Microgrid Based on Impedance Reshaping. *J. Mar. Sci. Eng.* **2024**, *12*, 503. https://doi.org/10.3390/jmse12030503

Academic Editor: Rafael Morales

Received: 26 January 2024
Revised: 12 March 2024
Accepted: 15 March 2024
Published: 18 March 2024

1. Introduction

Against the backdrop of "carbon peaking" and "carbon neutrality," distributed generation technology is increasingly being used in the grid, and microgrids have become an effective form of distributed generation technology. The development of ship microgrids using new energy technology is expected to achieve energy conservation and emission reduction goals in the maritime industry [1,2].

Depending on the electrical system, ship microgrids can be classified into AC and DC. In comparison to AC microgrids, DC microgrids exhibit prominent advantages, such as high efficiency, a low cost, and high reliability [3–5]. However, with the penetration of electronic devices and the negative impedance characteristics of constant power loads, ship DC microgrid systems are becoming less stable [6–8]. This mainly includes the rotor angle stability of the generator and the DC bus voltage stability. With the introduction of asynchronous generators, rotor angle stability has been effectively addressed, allowing us to focus more on the stability of the DC bus voltage. In this field, both domestic and international scholars have conducted extensive research, aiming to solve this complex and crucial problem.

Currently, research on the stability of ship DC microgrids primarily involves mechanism modeling and selecting effective control theories to analyze the local stability of the

system. This can be categorized into large- and small-signal stability analyses [9]. The common methods used in small-signal analysis include eigenvalue and impedance analyses, the Routh–Hurwitz criterion, etc. [10–12]. To further enhance the stability of DC microgrid systems, other researchers have proposed various control optimization techniques that are categorized mainly into passive and active damping control technologies [13].

Passive damping technology is primarily achieved by adding passive components (such as resistors, inductors, or capacitors) to the converter ports. However, passive damping solutions increase the systems' costs, reduce the power density, and lack adaptability and flexibility [14–16]. Therefore, passive damping technology is not suitable for DC microgrids. Active damping technology, on the other hand, modifies the control loop of the converter via the serial or parallel connection of virtual impedances to maintain power balance on the power source and load sides, stabilize the DC bus voltage, and increase the stability margin of the system. In reference [17], a first-order low-pass filter in series with a droop loop effectively suppressed high-frequency oscillations in the DC bus voltage caused by constant power loads. The authors of reference [18] employed parallel virtual impedance to suppress high-frequency oscillations in the DC bus voltage, achieving a good stability margin for the system. The authors of reference [19] proposed an advanced power management system (PMS) to reconfigure the control parameters, executing control tuning by integrating the PMS, thereby maintaining system stability without any load shedding, sustaining dynamic performance, and extending the flexibility and resilience of regional DC grid operation. Building upon [19], the authors of reference [20] further addressed the issue of configuring the PMS after predicting unstable conditions by implementing a weighted bandwidth method (WBM). By adjusting the control gains to ensure that the stable power distribution is unaffected by the system configurations, they verified the reconfiguration algorithm's capability through real-time platform C-HIL testing.

However, when the power converter is not under closed-loop control, the traditional series and parallel virtual impedance schemes fail to address this issue. Therefore, scholars at home and abroad have conducted in-depth research on methods to control the bus voltage stability of DC microgrids using impedance reshaping. The authors of reference [21] established a detailed impedance model, considering the influences of grid impedance and control delay, analyzed the main factors leading to enhanced negative damping effects and high-frequency resonance in voltage source converters (VSCs), and proposed a coordinated reshaping approach using this analysis, effectively suppressing the high-frequency resonance caused by high-frequency negative damping. The authors of reference [22] proposed an impedance reshaping control method that extracts the dynamic components of grid voltage, compensates for the power output accordingly, coordinates power output regulation, and neutralizes voltage dynamics in the power flow direction, thereby stabilizing the bidirectional power flow and grid-side voltage. Experimental verification has demonstrated the correctness and feasibility of this method.

In summary, although methods have been proposed to address the instability issue of the DC bus voltage caused by constant power negative impedance at the load side, DC microgrid systems feature multiple types of power sources and converters, each with unique characteristics and behaviors. This complexity and unpredictability significantly increase the challenges of system dynamics and stability. In such scenarios, achieving comprehensive impedance modeling and stability analysis of the entire system becomes a crucial and challenging task, considering the characteristics of various types of power sources and converters as well as their interactions and coupling effects.

Therefore, to address the DC bus voltage instability caused by constant power, negative impedance on the load side, this paper proposes an impedance magnitude reshaping method using bus voltage feedback based on the power-source-side impedance reshaping theory. This paper provides a detailed design approach for the impedance regulator parameters, models the reshaped system using MATLAB R2022a/Simulink, performs stability comparative analysis, and finally validates the method on a semi-physical simulation

platform. The research results indicate that this method effectively increases the stability margin of the DC bus voltage and stabilizes the DC microgrid.

2. Lithium Battery Energy Storage Unit Output Impedance Model

A schematic diagram of the ship DC microgrid studied in this paper is shown in Figure 1. This system is primarily composed of a diesel engine unit, an asynchronous generator unit, a lithium battery energy storage unit, a main propulsion load unit, and an auxiliary load unit. These components are connected to the DC bus through power electronic converters.

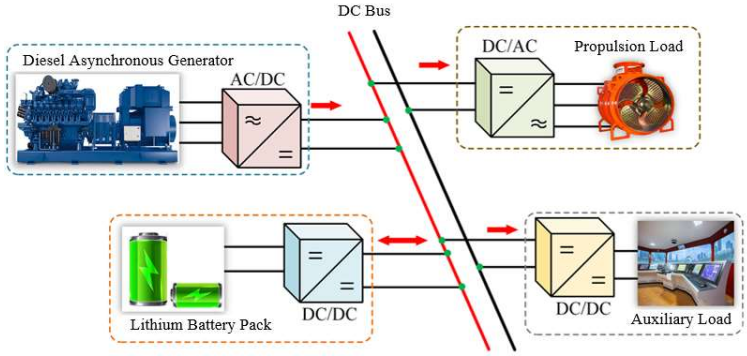

Figure 1. Schematic diagram of ship DC microgrid topology (Red arrows: Direction of internal power flow within the system. Red/Black lines: Positive and negative lines of the DC busbar. Green dots: Connection points on the DC busbar where diesel generator sets, lithium battery packs, propulsion loads, and auxiliary loads are interfaced via converters).

Given the significant impact of the lithium battery energy storage unit on system stability [23], the primary task is to accurately and mathematically model the output impedance of the lithium battery. The bidirectional DC/DC converter of the lithium battery energy storage unit adopts a droop control strategy with dual voltage and current closed loops. When the load side is in high-power mode, energy flows from the power source side to the load side. Therefore, we analyze the Boost operation mode of this bidirectional DC/DC converter as an example. Its circuit topology and control structure are shown in Figure 2.

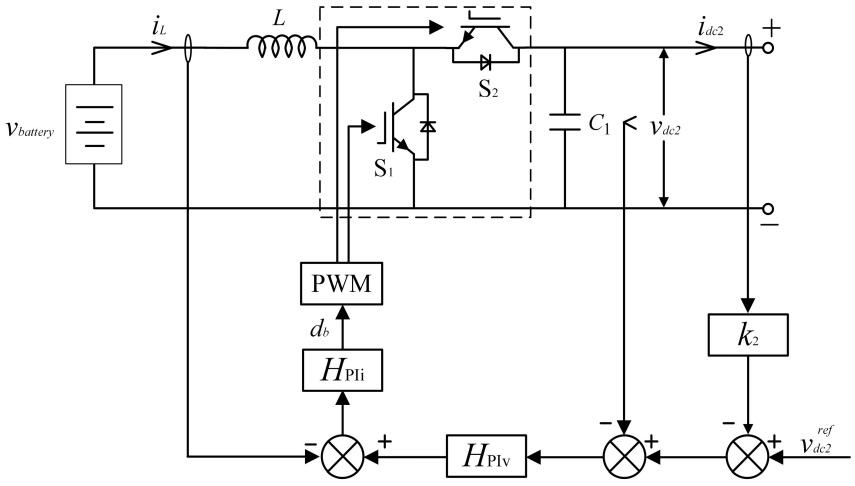

Figure 2. Circuit topology and control structure of a lithium battery energy storage unit.

In the diagram, v_{dc2}^{ref} represent the reference value for the output voltage of the bidirectional DC/DC converter; v_{dc2} and i_{dc2} represent the actual output voltage and current of the bidirectional DC/DC converter, respectively; $v_{battery}$ and i_L denote the input voltage

and current of the bidirectional DC/DC converter; L and d_b represent the filtering inductance and duty cycle of the bidirectional DC/DC converter, respectively; C_1 is the output capacitance of the bidirectional DC/DC converter; H_{Plv} and H_{Pli} represent the transfer functions of the voltage and current loop PI controllers, respectively; and k_2 denotes the droop coefficient.

A mathematical model of the bidirectional DC/DC converter of the lithium battery energy storage unit is established using Figure 2.

$$\begin{cases} L\frac{di_L}{dt} = v_{battery} - d_b v_{dc2} \\ C_1\frac{dv_{dc2}}{dt} = d_b i_L - i_{dc2} \end{cases} \tag{1}$$

Small disturbances are applied to the mathematical model of the bidirectional DC/DC converter in the lithium battery energy storage unit (Δi_L, Δi_{dc2}, Δv_{dc2}, $\Delta v_{battery}$, and Δd_b). By neglecting the second-order disturbance component, the small-signal mathematical model of the bidirectional DC/DC converter in the lithium battery energy storage unit can be represented as follows:

$$\begin{cases} L\frac{d\Delta i_L}{dt} = \Delta v_{battery} - R_L\Delta i_L - (1-D_b)\Delta v_{dc2} + v_{dc2}\Delta d_b \\ C_1\frac{d\Delta v_{dc2}}{dt} = (1-D_b)\Delta i_L + I_L\Delta d_b - \Delta i_{dc2} \end{cases} \tag{2}$$

In this equation, Δv_{dc2} represents the steady-state value of the output voltage of the bidirectional DC/DC converter at the operating point. I_L represents the steady-state value of the current through the output voltage filtering inductor of the bidirectional DC/DC converter at the operating point. D_b represents the steady-state value of the duty cycle of the bidirectional DC/DC converter at the operating point.

To convert the time-domain small-signal mathematical model expression of the bidirectional DC/DC converter in the lithium battery energy storage unit into a frequency-domain small-signal model, we use the following equation:

$$\begin{cases} sL\Delta i_L = \Delta v_{battery} - R_L\Delta i_L - (1-D_b)\Delta v_{dc2} + v_{dc2}\Delta d_b \\ sC_1\Delta v_{dc2} = (1-D_b)\Delta i_L + I_L\Delta d_b - \Delta i_{dc2} \end{cases} \tag{3}$$

Matrix operations are performed using Equation (3) to solve the transfer function expressions between various disturbance quantities of the bidirectional DC/DC converter in the lithium battery energy storage unit, as shown in Equations (4) to (9).

The transfer from the lithium battery terminal voltage $\Delta v_{battery}$ to the inductor current Δi_L of the bidirectional DC/DC converter in the lithium battery energy storage unit is represented as follows:

$$H_{iv}(s) = \frac{\Delta i_L}{\Delta v_{battery}} = \frac{C_1 s}{C_1 L s^2 + C_1 R_L s + (1-D_b)^2} \tag{4}$$

The transfer from the lithium battery terminal voltage $\Delta v_{battery}$ to the DC bus-side output voltage Δv_{dc2} of the bidirectional DC/DC converter in the lithium battery energy storage unit is represented as follows:

$$H_{vv}(s) = \frac{\Delta v_{dc2}}{\Delta v_{battery}} = \frac{1-D_b}{C_1 L s^2 + C_1 R_L s + (1-D_b)^2} \tag{5}$$

The transfer from the DC bus-side output current i_{dc2} to the inductor current Δi_L of the bidirectional DC/DC converter in the lithium battery energy storage unit is represented as follows:

$$H_{ii}(s) = \frac{\Delta i_L}{\Delta i_{dc2}} = \frac{1-D_b}{C_1 L s^2 + C_1 R_L s + (1-D_b)^2} \tag{6}$$

The transfer from the DC bus-side output current Δi_{dc2} to the DC bus-side output voltage Δv_{dc2} of the bidirectional DC/DC converter in the lithium battery energy storage unit is represented as follows:

$$H_{vi}(s) = \frac{\Delta v_{dc2}}{\Delta i_{dc2}} = -\frac{Ls}{C_1 Ls^2 + C_1 R_L s + (1 - D_b)^2} \tag{7}$$

The transfer from the duty cycle Δd_b to the inductor current Δi_L of the bidirectional DC/DC converter in the lithium battery energy storage unit is represented as follows:

$$H_{id}(s) = \frac{\Delta i_L}{\Delta d_b} = \frac{-C_1 V_{dc2} s - (1 - D_b) I_L}{C_1 Ls^2 + C_1 R_L s + (1 - D_b)^2} \tag{8}$$

The transfer from the duty cycle Δd_b to the DC bus-side output voltage Δv_{dc2} of the bidirectional DC/DC converter in the lithium battery energy storage unit is represented as follows:

$$H_{vd}(s) = \frac{\Delta v_{dc2}}{\Delta d_b} = \frac{I_L Ls - (1 - D_b) V_{dc2}}{C_1 Ls^2 + C_1 R_L s + (1 - D_b)^2} \tag{9}$$

According to the transfer function expressions between various disturbance quantities of the bidirectional DC/DC converter in the lithium battery energy storage unit, a small-signal control block diagram for the lithium battery energy storage unit DC/DC converter is established, as shown in Figure 3.

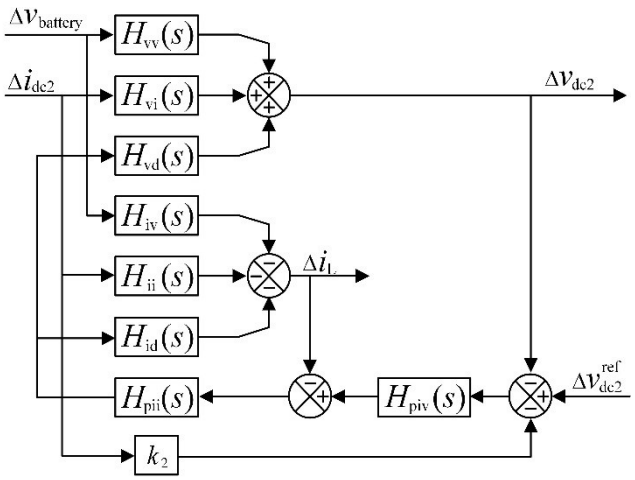

Figure 3. Small-signal control block diagram of the lithium battery energy storage unit bidirectional DC/DC converter.

In which, $H_{piv}(s)$ and $H_{pii}(s)$ represent the transfer functions of the voltage and current loop PI controllers for the bidirectional DC/DC converter in the lithium battery energy storage unit, and their expressions are as follows:

$$\begin{cases} H_{piv}(s) = k_{pv2} + \frac{k_{iv2}}{s} \\ H_{pii}(s) = k_{pi2} + \frac{k_{ii2}}{s} \end{cases} \tag{10}$$

In which, k_{pv2} and k_{iv2} represent the proportional and integral coefficients of the voltage loop PI controller for the bidirectional DC/DC converter in the lithium battery energy storage unit; k_{pi2} and k_{ii2} represent the proportional and integral coefficients of the current loop PI controller for the same converter.

The small-signal control block diagram of the bidirectional DC/DC converter in the lithium battery energy storage unit is simplified, as shown in Figure 3, and an expression for the closed-loop output impedance of the lithium battery energy storage unit is obtained.

$$Z_{out2}(s) = -\frac{\Delta v_{dc2}}{\Delta i_{dc2}} = \frac{k_2 B_2(s) H_{piv}(s) + B_2(s) H_{ii}(s) - H_{vi}(s)}{1 + B_2(s) H_{piv}(s)} \tag{11}$$

In this equation, $B_2(s)$ represents the closed-loop transfer function of the current inner loop for the bidirectional DC/DC converter in the lithium battery energy storage unit, and its expression is as follows:

$$B_2(s) = \frac{H_{pii}(s) H_{vd}(s)}{1 + H_{pii}(s) H_{id}(s)} \tag{12}$$

3. Voltage Feedback-Based Impedance Reshaping Control Optimization Method

In a DC microgrid, when the equivalent output impedance on the power source side and input impedance on the load side intersect, failing to meet the impedance ratio Nyquist stability criterion, it leads to instability in the DC bus voltage. Therefore, employing impedance reshaping as a method to optimize the system control structure can stabilize the system. According to the impedance stability analysis theory, an equivalent impedance model of the DC microgrid is obtained, as shown in Figure 4.

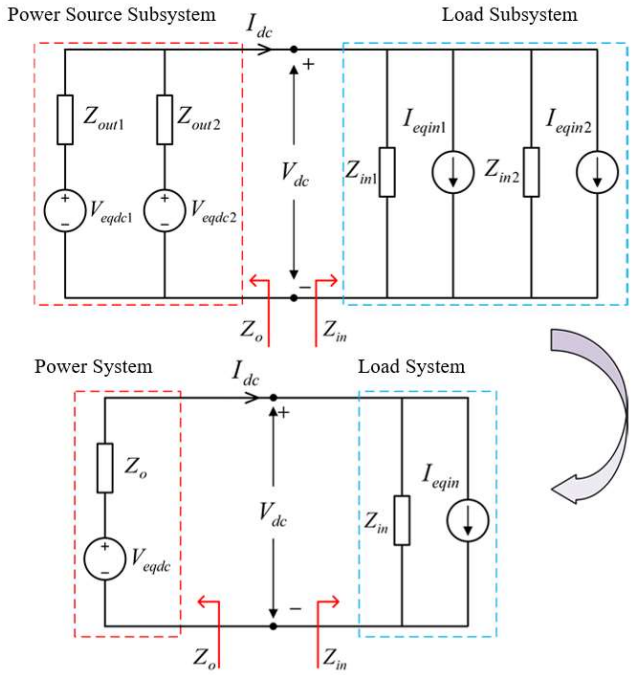

Figure 4. Equivalent impedance model of a DC microgrid.

By connecting the virtual impedances on the DC bus side of the bidirectional DC/DC converter in the lithium battery energy storage unit in parallel, the output impedance of the lithium battery energy storage unit is reshaped, thereby impacting the equivalent output impedance on the power source side. An equivalent impedance model of the DC microgrid after impedance reshaping is shown in Figure 5. The green and blue dotted boxes represent the power source subsystem and the load subsystem, respectively.

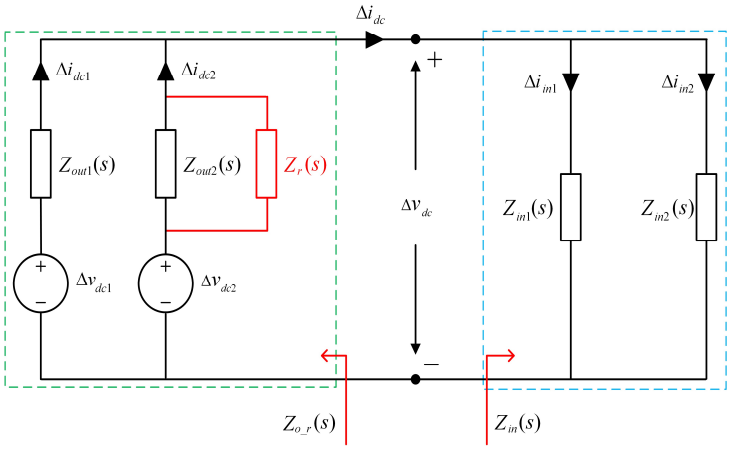

Figure 5. Equivalent impedance model of a DC microgrid after impedance reshaping.

Figure 6 shows a small-signal control block diagram of the bidirectional converter in the lithium battery energy storage unit after impedance reshaping, where $R(s)$ represents the output impedance regulator.

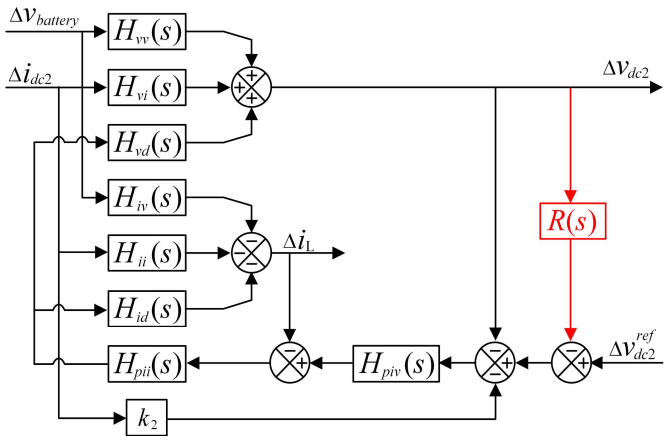

Figure 6. Small-signal control block diagram of the bidirectional DC/DC converter after impedance reshaping.

Figure 6 is simplified to derive an expression for the closed-loop output impedance $Z_{out2\_r}(s)$ of the bidirectional DC/DC converter after impedance reshaping. This is then rewritten in the admittance form, as shown in Equation (13).

$$\frac{1}{Z_{out2\_r}(s)} = \frac{1 + B_2(s)H_{piv}(s) + R(s)B_2(s)H_{piv}(s)}{k_2B_2(s)H_{piv}(s) + B_2(s)H_{ii}(s) - H_{vi}(s)} \tag{13}$$

Equation (13) is reorganized to obtain Equation (14).

$$\frac{1}{Z_{out2\_r}(s)} = \frac{1}{Z_{out2}(s)} + \frac{1}{Z_r(s)} = \frac{1 + B_2(s)H_{piv}(s) + R(s)B_2(s)H_{piv}(s)}{k_2B_2(s)H_{piv}(s) + B_2(s)H_{ii}(s) - H_{vi}(s)} \tag{14}$$

According to Equation (14), the closed-loop output impedance of the bidirectional DC/DC converter in the reshaped lithium battery energy storage unit is obtained via the

parallel combination of the original impedance $Z_{out2\_r}(s)$ and the virtual impedance $Z_r(s)$, where the virtual impedance $Z_r(s)$ can be expressed as follows:

$$Z_r(s) = \frac{1}{R(s)} \times \underbrace{\frac{k_2 B_2(s) H_{piv}(s) + B_2(s) H_{ii}(s) - H_{vi}(s)}{B_2(s) H_{piv}(s)}}_{Q(s)} \tag{15}$$

where $Q(s)$ represents the inherent term for virtual impedance, which can be obtained based on the system parameters. Considering an ideal voltage source, the impedance is zero across all the frequency bands. To approximate a voltage source, the parameters of the impedance regulator $R(s)$ can be designed to approximately offset $Q(s)$. Through equivalent elimination, a constant amplitude virtual impedance $Z_r(s)$ can be obtained. Further adjusting the parameters of $Z_{out2\_r}(s)$ allows for the adjustment of closed-loop output impedance $Z_o(s)$ of the bidirectional DC/DC converter in the lithium battery energy storage unit, and consequently, the effective output impedance $R(s)$ on the power source side can be changed. To properly design the parameters of the impedance regulator $Q(s)$, it is necessary to analyze the Bode plot of $Q(s)$ under different load powers, as shown in Figure 7. From the Bode plot, it can be observed that the amplitude curve of J can always be approximated using a first-order high-pass filter in the range of 1–200 Hz.

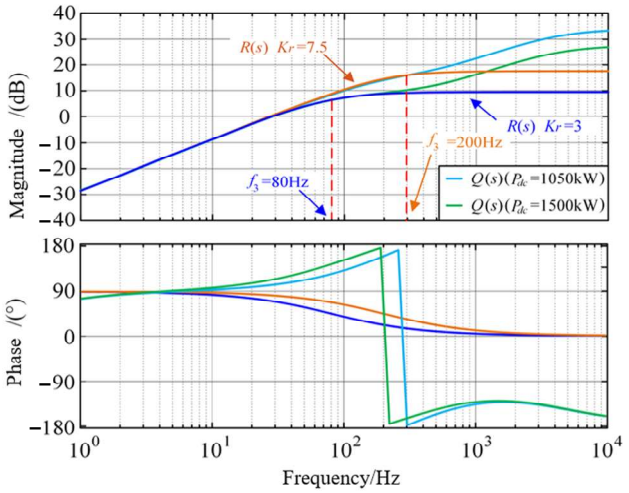

Figure 7. Bode plots of $Q(s)$ under different load powers.

Therefore, the transfer function of $R(s)$ is designed as follows:

$$R(s) = K_r \times \frac{s}{s + 2\pi f_3} \tag{16}$$

where K_r represents the gain coefficient of $R(s)$, and f_3 denotes the cutoff frequency of $R(s)$.

In order to approximate the virtual impedance expression $Z_r(s)$ as a fixed value in the range of 1–200 Hz for impedance reshaping, the cutoff frequency (f_3) of $R(s)$ is set to the value when the DC bus power (P_{dc}) is equal to 1050 kW. $R(s)$ corresponds to a cutoff frequency of 200 Hz. At this point, adjusting the gain coefficient K_r allows us to obtain virtual impedances $Z_r(s)$ with different amplitudes, as shown in Figure 8.

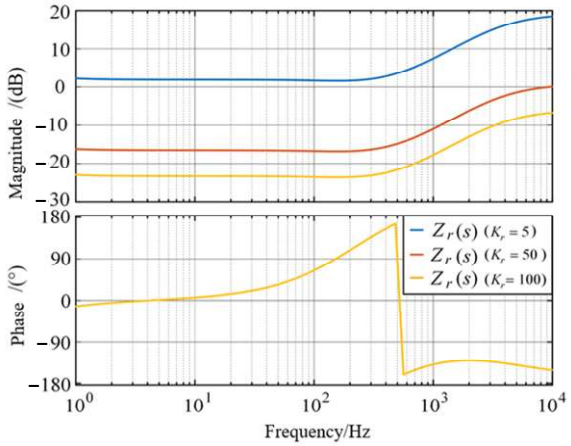

Figure 8. Bode plot showing the variation in the virtual impedance $Z_r(s)$ with different values of K_r.

From Figure 8, it can be seen that in the frequency range from 1 Hz to 200 Hz, the amplitude curve of the virtual impedance $Z_r(s)$ does not change with the frequency. Therefore, different amplitudes of $Z_r(s)$ can be obtained by adjusting K_r.

The Bode plot in Figure 9 illustrates the variation in the reshaped output impedance $Z_{out2\_r}(s)$ of the lithium battery energy storage unit with different values of K_r when P_{dc} is set to 1050 kW.

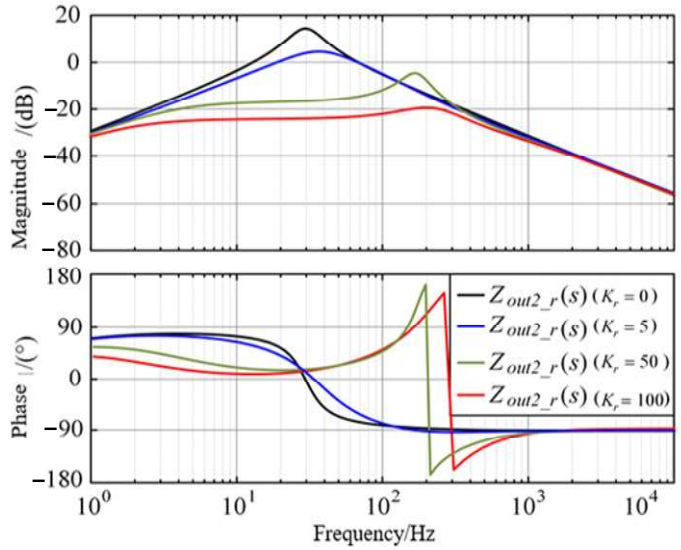

Figure 9. P_{dc} = 1050 kW; the Bode plot of $Z_{out2\_r}(s)$ with varying values of K_r.

From Figure 9, it can be observed that the amplitude of $Z_{out2\_r}(s)$ decreases with the increase in the gain coefficient K_r of the impedance adjuster $R(s)$, indicating that the impedance adjuster $R(s)$ can adjust the output impedance of the lithium battery energy storage unit.

The value of K_r is adjusted further to tune the amplitude curve of the reshaped equivalent output impedance $Z_{o\_r}(s)$ of the power source side, as shown in Figure 10.

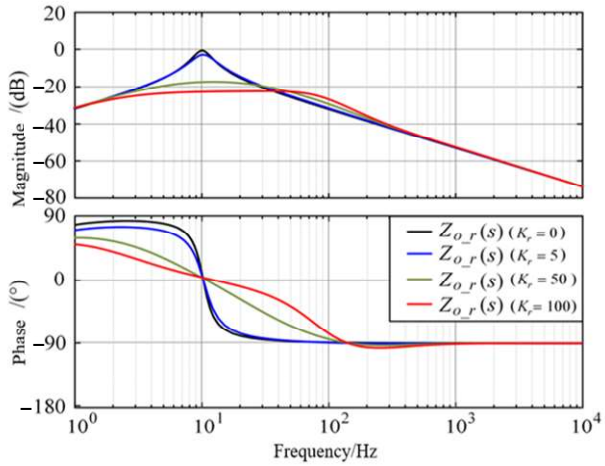

Figure 10. P_{dc} = 1050 kW; the Bode plot of $Z_{o\_r}(s)$ with varying values of K_r.

It can be observed that the amplitude curve of the reshaped equivalent output impedance $Z_{o\_r}(s)$ of the power source side decreases with the increase in the gain coefficient K_r of the impedance adjuster $R(s)$ in the frequency range of 2–40 Hz.

A Nyquist plot of $T_m(s)$ as a function of K_r after impedance reshaping is shown in Figure 11. From the graph, it can be observed that when K_r = 0, the impedance adjuster $R(s)$ has no effect. At this point, the Nyquist curve of the system $T_m(s)$ surrounds the point (−1, j0), indicating system instability. As the gain of the impedance adjuster K_r gradually increases, the Nyquist curve of $T_m(s)$ gradually moves away from the point (−1, j0), enhancing the stability margin of the system and improving the anti-interference capability of the DC bus voltage.

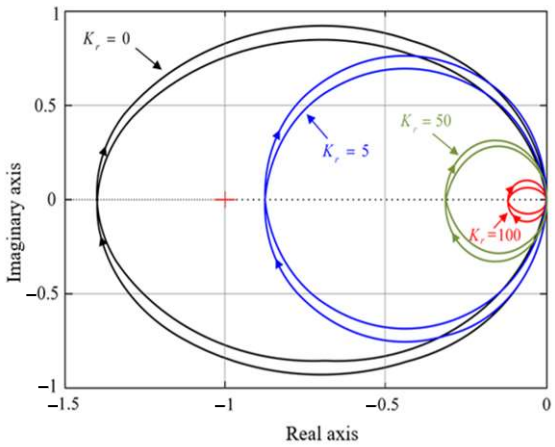

Figure 11. P_{dc} = 1050 kW; Nyquist plot of $T_m(s)$ with respect to K_r variations.

Therefore, the impedance reshaping control optimization method based on bus voltage feedback can reshape the amplitude curve of the equivalent output impedance on the power side of the DC microgrid in hybrid propulsion tugboats. A step-by-step diagram of the impedance reshaping method based on bus voltage feedback can be obtained through organization, as shown in Figure 12.

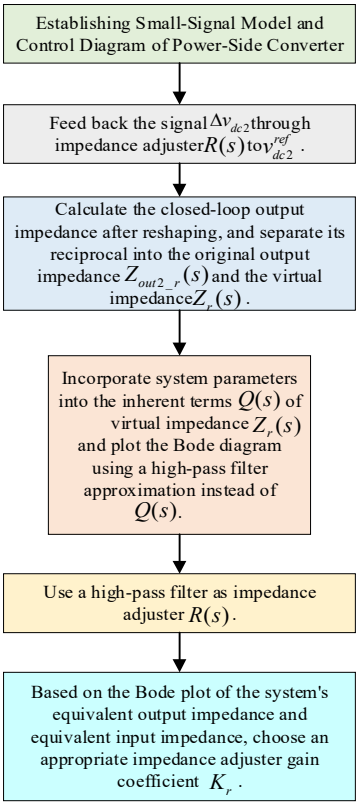

Figure 12. Implementation of an impedance reshaping control optimization method based on bus voltage feedback.

4. Simulation Validation

The simulation model of a DC microgrid in MATLAB/Simulink is built, setting the impedance adjuster K_r to 50 and 100, respectively. f_3 = 200 Hz. Simulation validation of the proposed impedance reshaping method is then performed.

4.1. Analysis of Voltage Stability for a Direct Current (DC) Bus with P_{dc} Set to 1050 kW

For P_{dc} = 1050 kW, the waveform of the DC bus voltage is shown in Figure 13 for different values of K_r, where K_r = 0 indicates that no impedance regulator is added, and traditional PID control is used for regulation. At 5 s, when a sudden 1050 kW load is applied to the propulsion system, the system impedance mismatch violates the impedance stability criterion, leading to oscillations in the DC bus voltage. At 6 s, when the lithium-ion battery energy storage unit converter is not connected to the impedance regulator, the DC bus voltage continues to oscillate. When the lithium-ion battery energy storage unit converter is connected to the impedance regulator, the DC bus voltage oscillation disappears, swiftly returning to a stable state. Comparing Figure 13a–c, it can be observed that by integrating the impedance regulator into the system, the oscillation of the DC bus voltage can effectively be eliminated, enhancing the system's capability to handle sudden load variations and improving its stability. Comparing Figure 13b,c, it is evident that when the coefficient K_r of the impedance adjuster is set to 50, the DC bus voltage recovers faster, but with an overshoot. On the other hand, when the coefficient K_r of the impedance adjuster is set to 100, the DC bus voltage recovers slower, and the overshoot is eliminated.

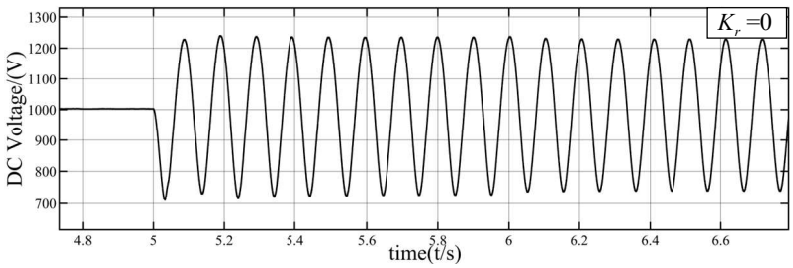

(**a**) K_r = 0; DC bus voltage waveform.

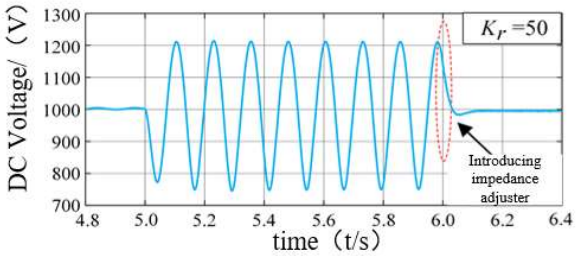

(**b**) K_r = 50; DC bus voltage waveform.

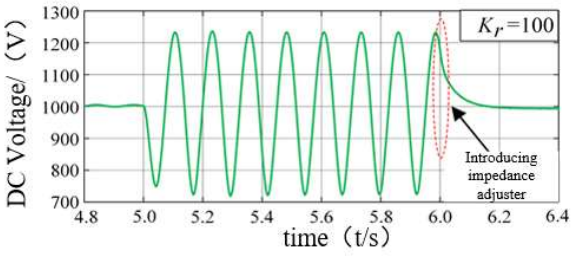

(**c**) K_r = 100; DC bus voltage waveform.

Figure 13. DC bus voltage waveforms are shown for different values of K_r.

4.2. Sudden Load Increase and Decrease Experiments

To verify the anti-interference ability of the DC bus voltage before and after impedance reshaping, comparative experiments are conducted, with the impedance regulator coefficient K_r set to 0 and 100, respectively. The voltage waveform under sudden load additions and removals at different power levels of the DC bus is shown in Figure 14. By comparing Figure 14a,b, it can be seen that, with the intervention of the impedance regulator, instantaneous voltage changes during load additions and removals are significantly reduced. Additionally, during the recovery process of the DC bus voltage, the original voltage oscillations are eliminated. This indicates that the introduction of the impedance regulator effectively stabilizes the DC bus voltage and further improves its anti-interference capability.

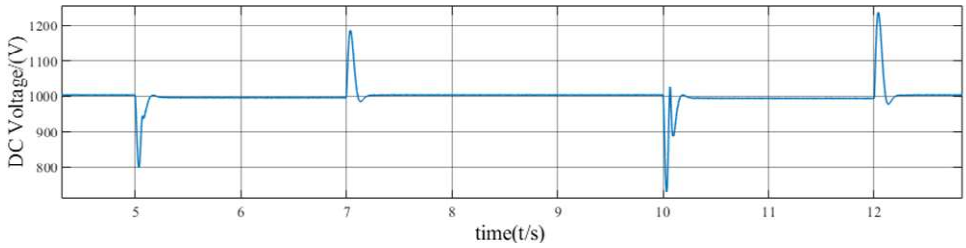

(**a**) Voltage waveform of the DC bus before impedance reshaping.

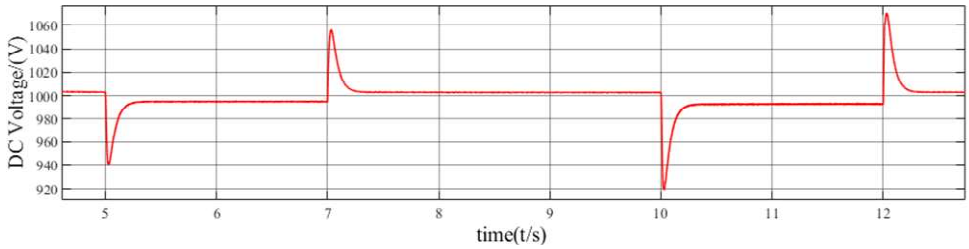

(**b**) Voltage waveform of the DC bus after impedance reshaping.

Figure 14. The voltage waveforms of the DC bus during sudden load additions and removals before and after impedance reshaping.

Based on the analysis of the DC bus voltage waveform, it can be observed that for different DC bus powers, when the DC bus voltage deviates due to impedance mismatching and fails to meet the stability criterion, the inclusion of an impedance regulator can significantly adjust the system's equivalent output impedance, restoring the DC bus voltage from an oscillatory state to a stable state.

It should be noted that deviations in the steady-state voltage of the DC bus are caused by droop control. The negative feedback mechanism of droop control requires the generator to adjust the output power based on the load demand. However, due to the limited response speed of the generator, it cannot immediately adjust the output power in response to load changes. Additionally, there is a delay in the response time of the DC voltage regulator. Therefore, droop control may cause transient voltage deviations when adjusting the generator's output power, thereby affecting the steady-state voltage of the DC bus. This is an inevitable drawback of droop control.

5. Experimental Verification

A semi-real simulation platform is built, as shown in Figure 15, to experimentally validate the proposed control optimization method.

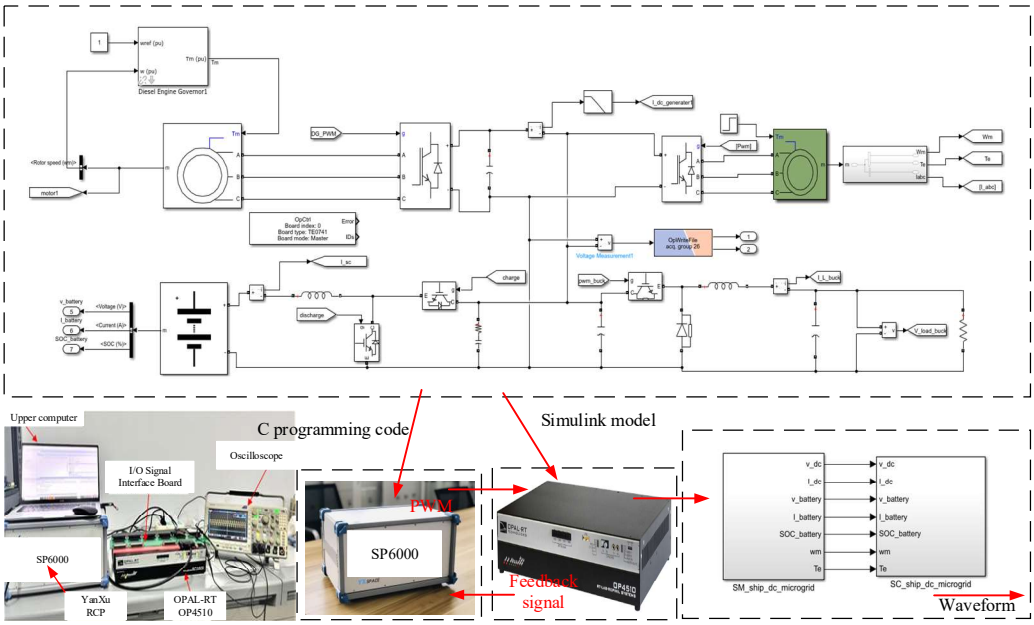

Figure 15. Semi-physical experiment platform for DC microgrid.

5.1. Under Different Operating Conditions, the Impedance Adjuster Suppresses DC Bus Oscillations

Figure 16 illustrates the damping effect of the impedance adjuster on DC bus oscillations under different operating conditions. In Figure 16a, with the impedance adjuster K_r = 100, when the DC bus power surges from 100 kW to 1050 kW, the DC bus voltage starts to oscillate. After introducing the impedance adjuster, the DC bus voltage oscillations disappear, returning to a stable state. In Figure 16b, with the impedance adjuster K_r = 100, when the DC bus power surges from 100 kW to 1500 kW, the DC bus voltage begins to oscillate, and the amplitude is slightly larger than that shown in Figure 16a. Subsequently, with the impedance adjuster, the DC bus voltage oscillations vanish, returning to a stable state.

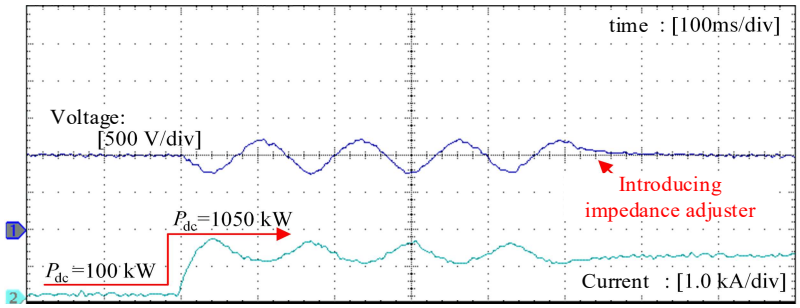

(**a**) When the DC bus power is 1050 kW, the impedance adjuster is introduced.

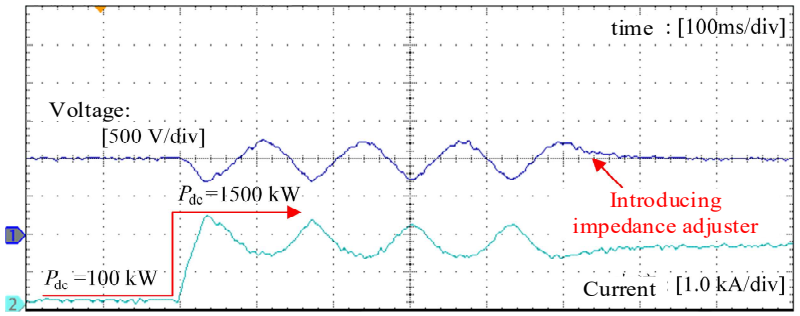

(**b**) When the DC bus power is 1500 kW, the impedance adjuster is introduced.

Figure 16. The damping effect of the impedance adjuster on DC bus oscillations under different operating conditions.

The experimental results indicate that setting the value of the impedance adjuster K_r to 100 can provide the system's DC bus voltage with a greater stability margin. Therefore, under different operating conditions, the impedance adjuster can effectively suppress DC bus oscillations. These results are consistent with the impedance reshaping theory and simulation analysis.

5.2. DC Bus Sudden Load Addition and Removal Experiments

In Figure 17, the experimental results of sudden load addition and removal on the DC bus of a hybrid propulsion tugboat with an impedance adjuster K_r = 100 are presented. From Figure 17a, it can be observed that after the introduction of the impedance adjuster, the DC bus power surges from 100 kW to 1050 kW, causing a 6% drop in the DC bus voltage, which then increases to 1000 V through adjustment. During sudden load removal, the DC bus voltage rises by 6%, stabilizing at 1000 V after a brief adjustment.

From Figure 17b, it can be observed that after the introduction of the impedance adjuster, the DC bus power surges from 100 kW to 1500 kW, causing a 9% drop in the DC bus voltage, which then increases to 1000 V through adjustment. During sudden load removal, the DC bus voltage rises by 8%, stabilizing at 1000 V after a brief adjustment. Therefore, by introducing the impedance adjuster to reduce the amplitude of the system's power-side output impedance, the interference resistance of the DC bus can be enhanced.

The analysis of the experimental results reveals that reshaping the amplitude of the system's power-side output impedance can effectively stabilize the DC bus voltage, reducing the fluctuations during sudden load addition and removal. The experimental outcomes align closely with our theoretical analysis and simulation results, validating the effectiveness of the proposed control optimization method.

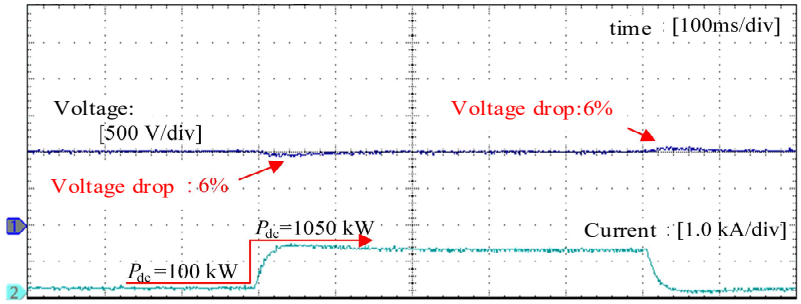

(**a**) Sudden addition and removal of a 1050 kW load on the DC bus.

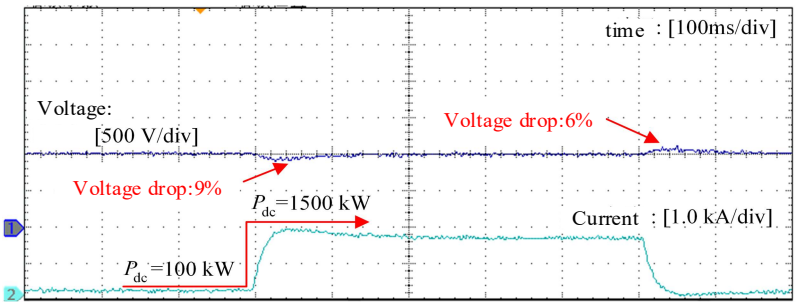

(**b**) Sudden addition and removal of a 1500 kW load on the DC bus.

Figure 17. The experimental results of sudden load addition and removal on the DC bus.

6. Conclusions

This paper delves into the issue of reshaping the power-side output impedance based on impedance reshaping principles. By introducing the concept of an impedance adjuster, a control optimization method for power-side impedance reshaping is proposed using bus voltage feedback as its foundation. Through theoretical analysis, simulation verification, and experimental validation, the following key conclusions are drawn:

1. Adopting a control optimization method based on impedance reshaping to optimize the system's power-side output impedance can effectively suppress DC bus voltage oscillations. The DC bus's voltage interference resistance can be further enhanced by adjusting the parameters of the impedance adjuster.
2. For different DC bus powers, when the DC bus voltage experiences an impedance mismatch, introducing an impedance adjuster can significantly adjust the equivalent output impedance, restoring the DC bus voltage from an oscillatory state to a stable state.
3. Reshaping the amplitude of the power-side output impedance in a DC microgrid system can effectively stabilize the DC bus voltage, reducing the fluctuations during sudden load addition and removal.

Author Contributions: Conceptualization, W.L. and R.Y.; methodology, Z.Q.; software, Z.Q. and X.D.; validation, Z.Q. and X.D.; writing—review and editing, Z.Q. and X.D.; supervision, W.L. All authors have read and agreed to the published version of the manuscript.

Funding: This paper was supported by the National Natural Science Foundation of China (52171308), the Natural Science Foundation of Fujian Province, China (2022J01333), and the Innovation Laboratory for Sciences and Technologies of Energy Materials of Fujian Province.

Institutional Review Board Statement: Not applicable.

Informed Consent Statement: Not applicable.

Data Availability Statement: The data presented in this article are available upon request from the first author.

Conflicts of Interest: The authors declare no conflicts of interest.

References

1. Zou, Z.; Wang, C.; Zhang, C.; Liu, S.; Liu, W. Linear power flow calculation of isolated island microgrid based on sag control. *Lab. Res. Explor.* **2022**, *41*, 124–129.
2. Li, S.; Li, J.; Dong, Y.; Shi, L.; Zhang, H.; Li, Y. Flexible Power Control and Voltage Suppression Strategy for Multi-sub-Microgrid AC-DC Hybrid Distribution System. *Electr. Power Autom. Equip.* **2021**, *41*, 99–106.
3. Tao, L.; Wang, P.; Wang, Y.; Ma, X.; Cheng, P. Parameter Optimization and Self-Disturbance Control of Low-Voltage Interface Converters in Microgrids. *J. Electr. Power Sci. Technol.* **2022**, *37*, 4202–4211. [CrossRef]
4. Zhang, W.; Zhang, H.; Zhi, N.; Wang, C.; Zeng, C. Control Strategy for Energy Storage Converter in DC Microgrid Based on Node Source-Load Current Differential. *J. Electr. Power Sci. Technol.* **2022**, *37*, 2199–2210. [CrossRef]
5. Xu, L.; Guerrero, J.M.; Lashab, A.; Wei, B.; Bazmohammadi, N.; Vasquez, J.C.; Abusorrah, A. A review of DC shipboard microgrids-part II: Control architectures, stability analysis, and protection schemes. *IEEE Trans. Power Electron.* **2022**, *37*, 4105–4120. [CrossRef]
6. Zhang, Z.; Song, G.; Zhang, X.; Zhou, J.; Wang, R. Stability and Robust Control Strategy of DC Microgrid Considering Constant Power Loads. *J. Electr. Power Sci. Technol.* **2023**, *38*, 4391–4405. [CrossRef]
7. Xie, W.; Han, M.; Yan, W.; Wang, C.; Yuan, D. Hierarchical Stability Control Strategy for DC Microgrid Considering Characteristics of Constant Power Loads. *J. Electr. Power Sci. Technol.* **2019**, *34*, 3430–3443. [CrossRef]
8. Hassan, M.A.; Su, C.L.; Pou, J.; Sulligoi, G.; Almakhles, D.; Bosich, D.; Guerrero, J.M. DC Shipboard Microgrids with Constant Power Loads: A Review of Advanced Nonlinear Control Strategies and Stabilization Techniques. *IEEE Trans. Smart Grid* **2022**, *13*, 3422–3438. [CrossRef]
9. Yuan, Y.; Wang, J.; Yan, X.; Shen, B.; Long, T. A review of multi-energy hybrid power system for ships. *Renew. Sustain. Energy Rev.* **2020**, *132*, 110081. [CrossRef]
10. Park, D.; Zadeh, M. Dynamic modeling, stability analysis, and power management of shipboard DC hybrid power systems. *IEEE Trans. Transp. Electrif.* **2021**, *8*, 225–238. [CrossRef]
11. Gao, J.; Qin, L. Modeling of Input Impedance and Stability Analysis for Virtual Synchronous Generator. *Power Syst. Technol.* **2021**, *45*, 578–588.
12. Wu, Q.; Deng, W.; Tan, J.; Sha, J.; Qin, X.; Yuan, W. Stability Analysis of Multi-Terminal DC Systems Based on Droop Control. *J. Electr. Power Sci. Technol.* **2021**, *36*, 507–516. [CrossRef]
13. Liu, X.; Yang, J.; Li, L.; Dong, M.; Song, D. Stability Detection of DC Microgrid System with Passive Damping Based on Machine Learning. *J. Electr. Power Sci. Technol.* **2024**, 1–14. [CrossRef]
14. Lorzadeh, O.; Lorzadeh, I.; Soltani, M.N.; Hajizadeh, A. Source-side virtual RC damper-based stabilization technique for cascaded systems in DC microgrids. *IEEE Trans. Energy Convers.* **2021**, *36*, 1883–1895. [CrossRef]
15. Hao, W.; Tan, W.; Huang, Y.; Sun, S.; Tang, J.; Du, X. Strategy for Suppressing High-Frequency Oscillations in Flexible DC Transmission Systems Based on Passive Damping. *Adv. Technol. Electr. Eng. Energy* **2023**, *42*, 23–31.
16. He, B.; Chen, W.; Li, X.; Shu, L.; Ruan, X. A power adaptive impedance reshaping strategy for cascaded DC system with buck-type constant power load. *IEEE Trans. Power Electron.* **2022**, *37*, 8909–8920. [CrossRef]
17. Rashidirad, N.; Hamzeh, M.; Sheshyekani, K.; Afjei, E. High-frequency oscillations and their leading causes in DC microgrids. *IEEE Trans. Energy Convers.* **2017**, *32*, 1479–1491. [CrossRef]
18. Zhang, X.; Ruan, X.; Zhong, Q.C. Improving the stability of cascaded DC/DC converter systems via shaping the input impedance of the load converter with a parallel or series virtual impedance. *IEEE Trans. Ind. Electron.* **2015**, *62*, 7499–7512. [CrossRef]
19. Tavagnutti, A.A.; Chiandone, M.; Bosich, D.; Sulligoi, G. A Stability-Aimed PMS for Shipboard Zonal DC Microgrids: The C-HIL Tests on Real-Time Platform. In Proceedings of the 2023 IEEE Electric Ship Technologies Symposium (ESTS), Alexandria, VA, USA, 1–4 August 2023; pp. 453–457.
20. Andrea, A.T.; Daniele, B.; Giorgio, S. Optimized Tuning for Flexible and Resilient Control of Zonal DC Microgrids on Ships. In Proceedings of the 2023 IEEE Power & Energy Society General Meeting (PESGM), Orlando, FL, USA, 16–20 July 2023.
21. Nian, H.; Yang, J.; Hu, B.; Jiao, Y.; Xu, Y.; Li, M. Stability Analysis and Impedance Reshaping Method for DC Resonance in VSCs-based Power System. *IEEE Trans. Energy Convers.* **2021**, *36*, 3344–3354. [CrossRef]
22. Liu, L.; Wang, K.; Peng, F.; Tian, Y.; Wang, Y. Dynamic Grid Voltage-Based Impedance-Reshaped Control for the Stability Enhancement of Grid-Connected DC/AC Converter System under Bidirectional Power Flow. *Energies* **2022**, *15*, 7269. [CrossRef]
23. Qiao, Z.; Yang, R.; Liao, W.; Yu, W.; Fang, Y. Impedance modeling, Parameters sensitivity and Stability analysis of hybrid DC ship microgrid. *Electr. Power Syst. Res.* **2024**, *226*, 109901. [CrossRef]